Computational Study of the One- and Two-Photon Absorption and Circular Dichroism of L-Tryptophan

Maxime Guillaume* and Kenneth Ruud

Centre for Theoretical and Computational Chemistry, Department of Chemistry, University of Tromsø, N-9037 Tromsø, Norway

Antonio Rizzo and Susanna Monti

Istituto per i Processi Chimico-Fisici del Consiglio Nazionale delle Ricerche (IPCF-CNR), Area della Ricerca, via G. Moruzzi 1, I-56124 Pisa, Italy

Zijing Lin and Xuee Xu

Hefei National Laboratory for Physical Sciences at the Microscale, University of Science and Technology of China, and Department of Physics, University of Science and Technology of China, Hefei, Anhui 230026, China

Received: January 18, 2010

A density functional theory (DFT) study of the one- and two-photon absorption and circular dichroism spectra of L-tryptophan in water is presented. The effects on the simulated spectra of conformational averaging, of solvent as described by the polarizable continuum model (PCM), and of the choice of exchange-correlation (XC) functional are analyzed. Conformational Maxwell−Boltzmann (MB) averaging is carried out at room temperature in the gas phase using the ten lowest-energy conformers in the gas phase, whereas in the solvent, the nine lowest zwitterionic conformers are determined in combination with a PCM continuum model and employed in the calculations. One- and two-photon absorption and circular dichroism spectra are calculated using time-dependent DFT with both the B3LYP and CAM-B3LYP XC functionals, including the 15 lowest excited electronic states in each case. The spectra are shown to be strongly influenced by all parameters of our computational models. Changing the XC functional yields large changes not only in the excitation energies but also in the transition dipole moments and the rotational strengths of each excited state. The inclusion of the effect of water solvation also yields different response properties for each excited state, as well as different ground-state equilibrium geometries for the gas and solvated phases. MB weights change significantly from the gas to the solvated phase, making the effect of conformational averaging strongly phase dependent. The study of all these effects highlights the importance of an accurate and reliable treatment of both ground and excited states when aiming at predicting experimental one- or two-photon spectra. However, the comparison between the MB weighted spectra and experiment for the linear spectroscopies turns out to be rather satisfactory, showing that our approach can yield at least information on the major features of the spectra.

I. Introduction

Among all the spectroscopic approaches available to study the structure of molecular and biomolecular systems, an important role is taken by enantioselective methods which are able to reveal the chirality of the systems. These can be used for the detection of enantiomers, for the analysis of the yield of synthetic procedures for chiral molecules, or for that of proteins through the study of their secondary structures. The determination of the specific optical activity of an individual amino acid gives insight into its structure, complementary to that obtained with other commonly used methods such as X-ray crystallography and nuclear magnetic resonance. Among the 20 natural amino acids, 19 are chiral, and they exist in living species in only one enantiomeric form, the left configuration (L-form). Enzymatic activity is also often related to the chirality of binding sites, cofactors, and target molecules.

Different experimental methods exist to study the chirality and the corresponding optical activity of molecules, and one of the most common is electron circular dichroism (ECD) spectroscopy.[1−3] ECD detects the differential absorption, arising from mixed electric and magnetic dipole interactions, of left (LCP) and right (RCP) circular polarized UV−visible light. Other methods are also becoming increasingly popular: vibrational circular dichroism (VCD), in which the polarized electromagnetic field corresponds to an infrared beam and which probes the vibrational levels of the molecular system,[4] or Raman optical activity (ROA),[5] arising from the difference of the intensity in Raman scattered LCP and RCP light. ECD, VCD, and ROA provide complementary information on the structure and energetics of the system in different frequency ranges. Moreover, ECD complements UV−visible absorption spectroscopy, VCD is a complement to IR spectroscopy and ROA to Raman spectroscopy.

The above-mentioned methods all belong to the class of linear spectroscopies. Using nonlinear spectroscopy, which has gathered increasing attention over the past few years, other types of transitions can be investigated. These phenomena imply

* Corresponding author. Current address: Laboratory for Chemistry of Novel Materials, University of Mons, Place du parc 20, 7000 Mons (Belgium). Tel.: +32-65-37-38-63. Fax: +32-65-37-38-61. E-mail: maxime.guillaume@umons.ac.be.

10.1021/jp1004659
Published on Web 04/26/2010

multiphoton transitions or scattering, leading to different selection rules with respect to the linear counterparts and therefore allowing in principle for the investigation of different electronic or vibrational states of molecules. Two-photon absorption (TPA) results from the coherent electronic excitation of a chromophore unit by two low-energy photons.[6−8] This spectroscopy has several potential advantages. For instance, the phenomenon can be focused on a three-dimensional section of the sample, which yields an accurate and local probing of chromophores, instead of a globally averaged signal over the whole medium as obtained in the linear UV−visible phenomenon.

The combination of TPA with circular polarization led Tinoco[9] in 1975 to predict and rationalize theoretically the nonlinear analogue of ECD, namely, two-photon circular dichroism (TPCD) corresponding to the differential two-photon absorption of LCP and RCP. Recently the use of response theory[10−12] was proposed for an efficient computational treatment of TPCD.[13,14] Using density functional theory (DFT) in combination with the hybrid Becke three-parameter exchange functional with the Lee−Yang−Parr correlation functional,[15−17] commonly denoted the B3LYP functional,[18] or with its long-range adapted Coulomb Attenuated Method-B3LYP (CAM-B3LYP)[19−22] variant, the TPCD response of systems with different characteristics (amino acids,[23] helicenes,[24] organic chromophores[25,26]) were studied, mostly in the gas phase. Recently, also vibronic effects on the TPCD spectra were investigated.[27]

From an experimental point of view, until very recently, attempts at detecting nonlinear circular dichroism have been scarce. The fluorescence-detected two-photon circular dichroism of uniaxial crystals of a Gadolinium complex was measured in 1995,[28,29] while at the turn of the millennium nonlinear circular dichroism induced by radiation was observed in liquid samples of ruthenium bipyridil salts.[30−34] Markowicz and co-workers established in 2004 upper limits for the two-photon dichroism that could be detected via a modified Z-scan technique.[35] A remarkable progress in experiment appears to be due to the work of Hernandez and co-workers, who developed recently a double L-scan technique,[36] yielding well-resolved TPCD and two-photon circular-linear dichroism (TPCLD,[37] the difference between circularly and linearly polarized TPA) spectra for solvated chiral samples. Using the L-scan experimental technique, the same group, in association with one of us, has recently published the first joint experimental and computational TPCD study on (*S*)-(−)-1,1′-bi(2-naphthol) and (*R*)-(+)-1,1′-bi(2-naphthol),[26] proving the feasibility of TPCD, its advantages in the understanding of optically active systems, and therefore the need to have a reliable support by theoretical approaches. The same authors have recently discussed the characteristics of the TPCLD response.[38]

In the present study, we aim at expanding on the analysis of ref 23 by studying the effects of solvation. For this purpose, the polarizable continuum model (PCM)[39−41] is employed in combination with response theory. The system under study is (L)-tryptophan, (L)-trp, which possesses a conjugated ring and which is known to play an important role in two-photon processes applied to biochemistry and protein spectroscopies.[42] In ref 23, the linear and nonlinear responses of (L)-trp were simulated on an isolated molecule, assuming a geometry taken from crystallographic data (see also ref 13).

The solvent considered in this work is water, and the scope of our analysis is to estimate the effects of solvation on the one-photon absorption (OPA), ECD, TPA, and TPCD spectra of (L)-trp by performing the simulation in both gas and solvent phases. Another important point of this study is the inclusion of conformational averaging effects, both in the gas phase and in the solvent. This is accomplished by analyzing the most stable conformers of (L)-trp both in the gas phase and in the solvent and by performing a Maxwell−Boltzmann (MB) averaging of the main contributions to both the absorption and circular dichroism spectra. The consequence of this is that in water the most stable conformers that are taken into account in the MB analysis are the zwitterionic structures, as these are stabilized by interactions with the polar solvent.[43]

A recent study[25] (see also refs 44, 45, and 27) has shown that some improvements can be expected in comparison with experiment when using the long-range adapted CAM-B3LYP functional.[19−22] In particular, the position and intensities of spectroscopic lines due to Rydberg-type and charge-transfer excitations could be obtained with an accuracy greater than that achieved with B3LYP. To what extent this effect can be expected to apply also to the case of (L)-trp is investigated in this study, by performing calculations with both the B3LYP and CAM-B3LYP exchange-correlation (XC) functionals.

The next two sections contain a brief introduction to the theory and the computational aspects of our study. The discussion of the main findings of this paper is split into two main parts. We first discuss the different effects on the OPA, ECD, TPA, and TPCD spectra of a single conformer of (L)-trp, the (energy-wise) lowest structure found in the gas phase, whose geometry is also reoptimized with PCM. A similar analysis of the effects of conformational averaging on the different spectra follows in the second part. We conclude the paper with a summary of the main findings and an outlook.

II. Theoretical Background

The quantity measured in linear absorption spectra is the molar absorptivity, which is related to the oscillator strength of each excited state and consequently to the transition dipole moment. For a transition from the ground $|0\rangle$ to an excited $|f\rangle$ electronic state, with $\hbar\omega_{0f} = E_f - E_0$, in an isotropic medium with refractive index $n \approx 1$, the following relationship between the molar absorptivity $\varepsilon^{\mathrm{OPA}}(\omega)$ and the oscillator strength f_{0f} exists

$$\varepsilon^{\mathrm{OPA}}(\omega) = \frac{2e^2\pi^2\omega N_A}{1000 \times \ln(10) \times (4\pi\varepsilon_0) \times m_e c_0} \times g(\omega, \omega_{0f}, \Gamma) \times \frac{f_{0f}}{\omega_{0f}} \quad (1)$$

$$= 1.05495 \times 10^3 \times \omega \times g(\omega, \omega_{0f}, \Gamma) \times \frac{f_{0f}}{\omega_{0f}} \quad (2)$$

where ω is the frequency of the radiation; $g(\omega, \omega_{0f}, \Gamma)$ is the normalized line shape, centered at $\omega = \omega_{0f}$ and with full width at half-maximum (FWHM) Γ (the product $\omega g(\omega)$ is unitless); N_A is Avogadro's number; c_0 is the speed of light in vacuo; and ε_0 is the electric constant. $f_{0f} = (2m_e\omega_{0f}|\mu_{0f}|^2)/(3\hbar^2e^2)$ is the oscillator strength of the $0 \rightarrow f$ transition, and it is given in terms of the transition matrix elements $(\mu_\alpha)^{0f} = \langle 0|\mu_\alpha|f\rangle$ of the electric dipole operator $\boldsymbol{\mu}$, whose component α is given as

$$\mu_\alpha = \sum_i q_i r_{i\alpha} \quad (3)$$

The summation involves the position r_i of all particles i of charge q_i. The electronic circular dichroism is defined as the

difference in the molar absorptivity $\varepsilon^{OPA}(\omega)$ for LCP and RCP light[2,9]

$$\Delta\varepsilon^{ECD}(\omega) = \varepsilon_L^{OPA}(\omega) - \varepsilon_R^{OPA}(\omega)$$

$$= \frac{64\pi^2\omega N_A}{9 \times 1000 \times \ln(10) \times (4\pi\varepsilon_0) \times \hbar c_0^2} \times g(\omega, \omega_{0f}, \Gamma) \times {}^fR \quad (4)$$

$$= 2.73719 \times 10^1 \times \omega \times g(\omega, \omega_{0f}, \Gamma) \times {}^fR \quad (5)$$

${}^fR$ is the ECD rotational strength,[1,2] which is given by the expression

$${}^fR = \frac{3}{4}\,\mathrm{Im}[\langle 0|\boldsymbol{\mu}|f\rangle \cdot \langle f|\mathbf{m}|0\rangle] \quad (6)$$

${}^fR$ involves the transition matrix elements of both the electric dipole $\boldsymbol{\mu}$ and of the magnetic $\mathbf{m}$ dipole operators, with

$$m_\alpha = \sum_i \frac{q_i}{2m_i} l_{i\alpha} = \sum_i \frac{q_i}{2m_i} (r_i \times p_i)_\alpha \quad (7)$$

Here the linear momentum $\boldsymbol{p}_i$, the angular momentum $\boldsymbol{l}_i$ operators, and the mass m_i of all particles i appear. Equations 2 and 5 give the observable in units of $dm^3\ mol^{-1}\ cm^{-1}$ starting from ω, ω_{0f}, and the rotational strength ${}^fR$ given in au (units of ${}^fR$: $e^2\hbar a_0 m_e^{-1}$).

In the dipole approximation, the two-photon absorption rate for two photons of equal frequency is usually written as[9,46] ($\hbar\omega_{0f} = 2\omega$)

$$\delta^{TPA} = \frac{1}{30}\frac{(2\pi)^3\omega^2 g(2\omega, \omega_{0f}, \Gamma)}{c_0^2(4\pi\varepsilon_0)^2} \times \left\{F\left[\sum_\rho S_{\rho\rho}^{0f}(\omega)\right]^2 + (G+H)\left[\sum_{\rho\sigma} S_{\rho\sigma}^{0f}(\omega) S_{\rho\sigma}^{0f}(\omega)\right]\right\}$$

$$= \frac{1}{30}\frac{(2\pi)^3\omega^2 g(2\omega, \omega_{0f}, \Gamma)}{c_0^2(4\pi\varepsilon_0)^2}\bar{\delta} \quad (8)$$

$$\approx 8.35150 \times 10^{-4} \times \omega^2 \times g(2\omega, \omega_{0f}, \Gamma) \times \bar{\delta} \quad (9)$$

where the tensor $S_{\alpha\beta}^{0f}(\omega_\beta)$ is defined as (considering the general case of $\omega_\alpha + \omega_\beta = \omega_{0f}$)

$$S_{\alpha\beta}^{0f}(\omega_\beta) = \frac{1}{\hbar}\sum_P \sum_{n\neq 0} \frac{(\mu_\alpha)^{0n}(\mu_\beta)^{nf}}{\omega_\alpha - \omega_{0n}} = \frac{1}{\hbar}\sum_{n\neq 0} \frac{(\mu_\alpha)^{0n}(\mu_\beta)^{nf}}{\omega_\alpha - \omega_{0n}} + \sum_{n\neq 0} \frac{(\mu_\beta)^{0n}(\mu_\alpha)^{nf}}{\omega_\beta - \omega_{0n}} \quad (10)$$

As clearly seen on the right side of eq 10, P permutes operators and associated frequencies. The F, G, and H parameters in eq 8 take different values for different polarization and propagation conditions of the two photons.[9,46]

TPCD[9] is defined as the differential absorption of two photons, of which at least one is circularly polarized. For two photons of equal frequency ω, the observable $\Delta\delta^{TPCD}(\omega) = \delta_L^{TPA}(\omega) - \delta_R^{TPA}(\omega)$ is[9,14]

$$\Delta\delta^{TPCD}(\omega) = \frac{4}{15}\frac{(2\pi)^3\omega^2}{c_0^3(4\pi\varepsilon_0)^2} \times g(2\omega, \omega_{0f}, \Gamma) \times {}^fR^{TPCD} \quad (11)$$

$$\approx 4.87555 \times 10^{-5} \times \omega^2 \times g(2\omega, \omega_{0f}, \Gamma) \times {}^fR^{TPCD} \quad (12)$$

where ${}^fR^{TPCD}$ is the TPCD rotational strength. In the formulation of Tinoco,[9] origin invariant results for the dichroism can be obtained independently of the completeness of the one-electron basis set employed in the calculation by using[14]

$${}^fR^{TPCD} = -b_1\mathscr{B}_1^{TI}(\omega) - b_2\mathscr{B}_2^{TI}(\omega) - b_3\mathscr{B}_3^{TI}(\omega) \quad (13)$$

$$\mathscr{B}_1^{TI}(\omega) = \frac{1}{\omega^3}\sum_{\rho\sigma} M_{\rho\sigma}^{p,0f}(\omega)\,\mathscr{P}_{\rho\sigma}^{p,f0*}(\omega) \quad (14)$$

$$\mathscr{B}_2^{TI}(\omega) = \frac{1}{2\omega^3}\sum_{\rho\sigma} \mathscr{T}_{\rho\sigma}^{+,0f}(\omega)\,\mathscr{P}_{\rho\sigma}^{p,f0*}(\omega) \quad (15)$$

$$\mathscr{B}_3^{TI}(\omega) = \frac{1}{\omega^3}\left[\sum_\rho M_{\rho\rho}^{p,0f}(\omega)\right]\left[\sum_\sigma \mathscr{P}_{\sigma\sigma}^{p,0f}(\omega)\right] \quad (16)$$

The tensors $\mathscr{P}_{\alpha\beta}^{p,0f}(\omega_\beta)$, $\mathscr{M}_{\alpha\beta}^{p,0f}(\omega_\beta)$, and $\mathscr{T}_{\alpha\beta}^{+,0f}(\omega_\beta)$ are defined by the following sum-over-state expressions

$$\mathscr{P}_{\alpha\beta}^{p,0f}(\omega_\beta) = \frac{1}{\hbar}\sum_P \sum_{n\neq 0} \frac{(\mu_\alpha^p)^{0n}(\mu_\beta^p)^{nf}}{\omega_\alpha - \omega_{0n}} \quad (17)$$

$$M_{\alpha\beta}^{p,0f}(\omega_\beta) = \frac{1}{\hbar}\sum_P \sum_{n\neq 0} \frac{(\mu_\alpha^p)^{0n}(m_\beta)^{nf}}{\omega_\alpha - \omega_{0n}} \quad (18)$$

$$\mathscr{T}_{\alpha\beta}^{+,0f}(\omega_\beta) = \frac{1}{\hbar}\varepsilon_{\beta\rho\sigma}\sum_P \sum_{n\neq 0} \frac{(T_{\alpha\rho}^{+})^{0n}(\mu_\sigma^p)^{nf}}{\omega_\alpha - \omega_{0n}} \quad (19)$$

Einstein summation over repeated indices (ρ and σ) is implied by the use of the Levi−Civita $\varepsilon_{\beta\rho\alpha}$ tensor in eq 19. Depending on the setup of the experiment (the polarization and the propagation of the beams), the parameters b_1, b_2, and b_3 take different values, as reported in ref 9. Among the operators appearing in eqs 17−19, the velocity operator $\boldsymbol{\mu}^p$

$$\mu_\alpha^p = \sum_i \frac{q_i}{m_i} p_{i\alpha} \quad (20)$$

and the mixed length−velocity form of the quadrupole operator[47] $\boldsymbol{T}^+$, defined as

$$T_{\alpha\beta}^{+} = \sum_i \frac{q_i}{m_i}(p_{i\alpha} r_{i\beta} + r_{i\alpha} p_{i\beta}) \quad (21)$$

TABLE 1: (L)-Tryptophan: Boltzmann Weights X_i (T = 298.15 K, P = 1 atm) for the Ten Lowest Conformers in the Gas Phase and for the Nine Lowest Zwitterionic Conformers in Water[a]

conformer	in the gas phase $100 \times X_i$	in water $100 \times X_i$
1	39.1 (1)	37.8
2	15.4 (4)	31.5
3	14.7 (5)	11.2
4	8.6 (2)	10.2
5	5.3 (3)	2.8
6	4.0 (7)	2.6
7	3.9 (6)	2.3
8	3.2 (8)	1.6
9	3.1 (10)	0.1
10	2.7 (9)	

[a] The reader should refer to the text for more details. Ordering of the conformers is done with respect to their weights. The labels associated for each conformer in the gas phase by Huang and Lin in ref 48 are given in parentheses.

also appear. Equations 9 and 12 yield the TPA and TPCD, respectively, in units of 10^{-50} cm^4 s molecule^{-1} photon^{-1} (GM), starting from the circular frequency ω, the line shape $g(2\omega, \omega_{0f}, \Gamma)$, the TPCD rotational strength ${}^fR^{\mathrm{TPCD}}$ (units: $e^4\, a_0^7\, m_e\, \hbar^{-3}$), and the TPA cross-section $\bar{\delta}$ (units: $e^4\, a_0^8\, m_e^2\, \hbar^{-4}$), all given in atomic units.

III. Computational Details

The structures of the ten most stable conformers of (L)-trp in the gas phase were taken from ref 48. Geometries were optimized at the B3LYP/6-311G(d) level, whereas the MB weights were obtained from energies at the MP2/6-311++G(d,p) level, added to relative zero-point vibrational energies obtained at the B3LYP/6-311G(d) level. Note that conformers were ordered here according to the MB weights, whereas they were labeled according to increasing MP2 energies in ref 48.

For the study of conformational effect in the solvent (water), the stable structures were determined as the following. A total of 108 trial structures were generated by allowing for all combinations of internal single-bond rotamers of zwitterionic tryptophan. The trial structures were first optimized at the BHandHLYP/6-31G(d) level of theory combined with the conductor-like polarization continuum model (CPCM).[49−53] A set of unique stable zwitterionic conformers thus obtained were reoptimized at the BHandHLYP/6-311+G(d,p) level with the CPCM model. Total energies were then calculated using MP2/6-311G(2df,p) electronic energies in combination with the CPCM model, whereas thermal corrections to the free energies at the standard state were obtained using BHandHLYP/6-311+G(d,p). A total of eleven zwitterionic conformers were obtained, but only nine of them were employed in this study, since for two of them the computed MB weight was found to be lower than 0.1%. MB weights for the ten gas phase conformers, and for the nine solvated zwitterionic forms employed in this study, are listed in Table 1, where also the correspondence between gas phase conformers in this paper and in ref 48 is given.

As a first step in the analysis, a structure optimization of a neutral conformer was carried out in water using the PCM[39−41] to model the effect of the water solvent (ε_∞ = 78.39, $\varepsilon_{\mathrm{opt}}$ = 1.776). The structure of conformer 1 of ref 48 was used as a starting guess for that optimization, carried out at the B3LYP level[15−17] using the aug-cc-pVDZ[54] basis set. The convergence criteria used during this geometry optimization in the solvent were set to 10^{-8} au for the energy and 10^{-6} au for the gradients. The two structures (the original gas phase and that optimized at the PCM level) were employed for the study discussed in Section IV.A below.

For the determination of the OPA, ECD, TPA, and TPCD spectra of each conformer, two different XC functionals were employed in association with the aug-cc-pVDZ basis set: B3LYP and CAM-B3LYP.[19,20] The latter was found recently to be particularly promising for studies of two-photon absorption processes[21] and was successfully used to predict the one- and two-photon response of gaseous and solvated *R*-(+)-3-methylcyclopentanone (R3MCP).[25,44,45,27] Here, as in these earlier studies, the standard formulation of CAM-B3LYP is exploited, with the fraction α of Hartree−Fock exchange in the case of short-range interaction set to 0.19, the additional fraction β of Hartree−Fock exchange introduced for long-range interaction equal to 0.46, and the interaction switching factor μ = 0.33.

All PCM calculations of the response properties for the OPA, ECD, TPA, and TPCD spectra were performed adopting a nonequilibrium solvation scheme.[55−57] For a detailed discussion on the reliability of PCM for the calculation of linear and nonlinear response properties, see refs 58−67.

The spectra were evaluated using response theory to determine the excitation energies ω_{0f} as the poles of the response functions, the transition moments $\langle 0|X_\alpha|n\rangle$ as single residues of the appropriate linear response function, and the two-photon tensors defined in eqs 10, 17, 18, and 19 as single residues of the relevant quadratic response functions.[10,11] For the computation of the linear ECD rotational strength ${}^fR$, the procedure of refs 68−70 was used, using London atomic orbitals[71] to ensure gauge-origin independent results. The two-photon rotational strength ${}^fR^{\mathrm{TP}}$ has been determined using the origin invariant "TI" formalism described by eq 8.[13,14]

The OPA, ECD, TPA, and TPCD spectra were generated using eqs 1, 4, 8, and 11, respectively, assuming Lorentzian line shape functions, $g(\omega, \omega_{0f}, \Gamma)$ and $g(2\omega, \omega_{0f}, \Gamma)$, normalized to unity in the frequency domain and with a FWHM Γ of 0.1 eV (between 2.5 and 7 nm in the 180−300 nm wavelength range of the spectra), except when a comparison is made with experiment, later in Section IV.A where the value of FWHM was increased to 0.3 eV (between 8 and 22 nm in our spectra). The results presented in the next section for the two-photon processes correspond to an experimental setup with two left circularly polarized beams of equal frequency propagating parallel to each other. For this arrangement, $b_1 = G + H = 6$ and $b_2 = -b_3 = -F = 2$.[9]

The Boltzmann-averaged spectrum was obtained at T = 298.15 K and a pressure P = 1 atm, using MB weights w_i—obtained as discussed at the beginning of this section—and the property $P_i(\omega)$ for each conformation i of the molecule, as follows

$$P^{\mathrm{avg}}(\omega) = \sum_{i=1,N_c} P_i(\omega) w_i \qquad (22)$$

where N_c indicates the number of conformers; N_c = 10 for the gas phase; and N_c = 9 for the water solution.

The geometry optimization of the gas phase and the zwitterionic structures has been realized using the Gaussian03 program package.[72]

All the property calculations were carried out using a development version of the parallelized[73,74] Dalton 2.0 electronic structure program.[75]

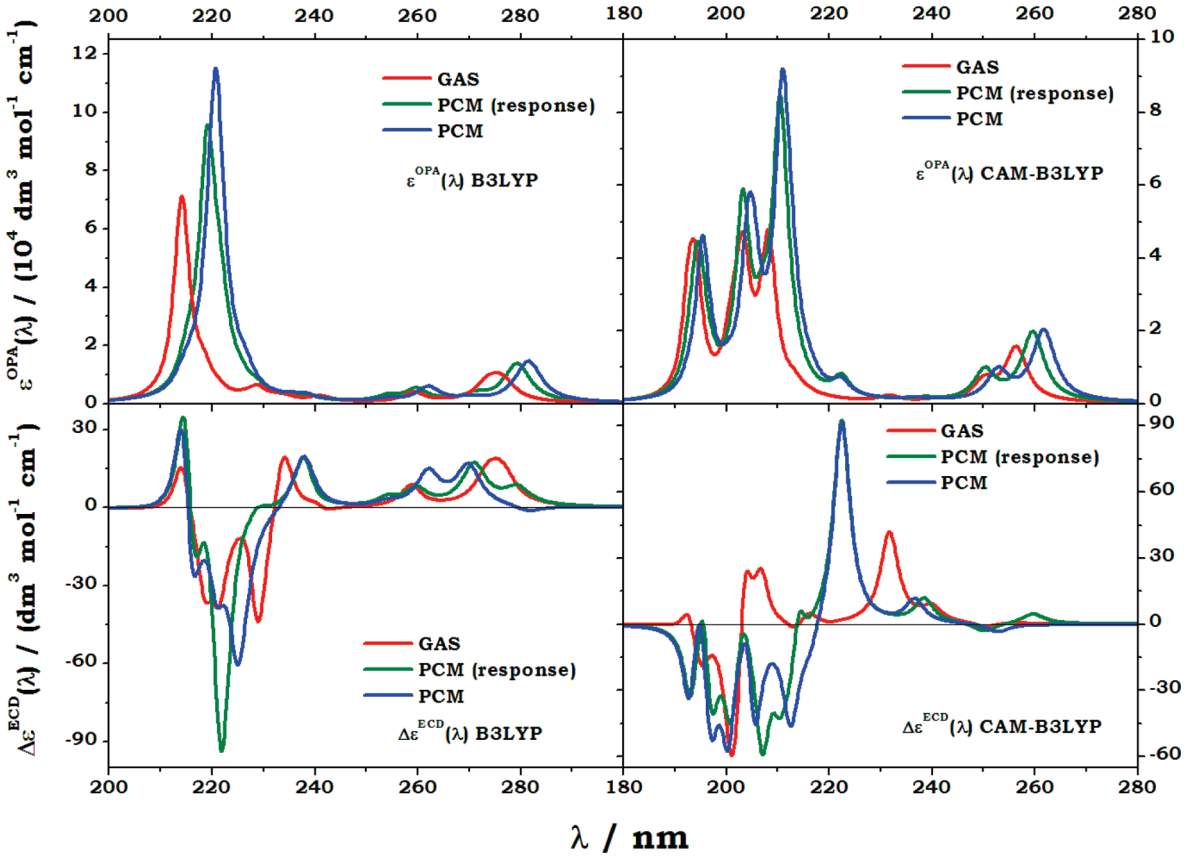

Figure 1. (L)-Tryptophan. OPA (top panels) and ECD (bottom panels) spectra of the lowest conformer, originally conformer 1 in ref 48, simulated in the range where the 15 lowest excited electronic states obtained using the aug-cc-pVDZ basis set with both B3LYP (left panels) and CAM-B3LYP (right panels) are located. Results are obtained in the gas phase ("GAS") and in water, using the polarization continuum model either for response properties only ("PCM(response)") or for both structure relaxation and response properties ("PCM").

IV. Results and Discussion

Our results will be presented in the two following sections. Section IV.A will focus on both the effects of the choice of XC functional (B3LYP or CAM-B3LYP) and of the inclusion of solvent—by comparing gas-phase simulations with those employing the PCM approach—on the OPA, ECD, TPA, and TPCD simulated spectra of (L)-trp. A comparison of the different combined approaches is done by focusing on the results obtained for a single conformer of (L)-trp, to estimate the different effects and their relative contributions. In Section IV.B, the effect of conformational averaging over the most stable neutral conformers of (L)-trp in the gas phase and over the most populated zwitterionic conformers in water solutions is made, to estimate the contribution of each effect on the simulation of the OPA, ECD, TPA, and TPCD spectra. As a measure of the reliability of our calculations, in Section IV.B we perform a comparison between our OPA and ECD spectra, simulated in water based on the Boltzmann weighted response of the zwitterionic conformers and the experimental spectra recorded by Auer.[76]

The data used for the analysis are available as Supporting Information,[77] where all the results obtained in this study for the relevant properties of interest, i.e., the oscillator strengths, the two-photon absorption cross sections, and the one- and two-photon rotatory strengths, are collected. Together with the excitation wavelengths, the relevant parameters introduced in Section III and contributing to the OPA, ECD, TPA, and TPCD responses are given for the most important conformers (vide infra), both for B3LYP and CAM-B3LYP. In all cases, the data refer to the lowest 15 excited electronic states.

A. Simulation of the Spectra of a Single (L)-trp Conformer: Solvent and XC Effects. The first part of this study concerns the analysis of the OPA, ECD, TPA, and TPCD spectra simulated for a single conformer of (L)-trp, using both the B3LYP and CAM-B3LYP functionals, both in the gas and in the solvent phases. The conformer used for this analysis is the most stable structure obtained from the conformational study in the gas phase, i.e., the one labeled conformer 1 in ref 48. Figures 1 and 2 show the simulated OPA, ECD, TPA, and TPCD spectra obtained using the B3LYP and CAM-B3LYP functionals, respectively. In each panel we compare the gas phase with the PCM results. Two different approaches were adopted when using PCM. In the first, the PCM model was applied for the calculation of the response properties using the gas-phase structure of conformer 1. The corresponding results are labeled "PCM (response)". In the second approach, conformer 1 was used as starting guess for further reoptimization in a continuum dielectric simulating the water phase, and the response properties were computed for the resulting solvent-optimized structure. These results are labeled "PCM" in Figures 1 and 2.

1. One-Photon Processes. The OPA and ECD spectra of the first conformer of (L)-trp are shown in the upper and lower panels of Figure 1, respectively, for B3LYP (left panels) and CAM-B3LYP (right panels). Each panel displays three spectra obtained for the gas phase, the PCM model associated with the gas phase structure, and the full solvent treatment, respectively. The data employed to prepare these figures are available in Table 1 of the Supporting Information. The range of wavelengths of Figure 1, from 180 to 300 nm, encompasses the region where

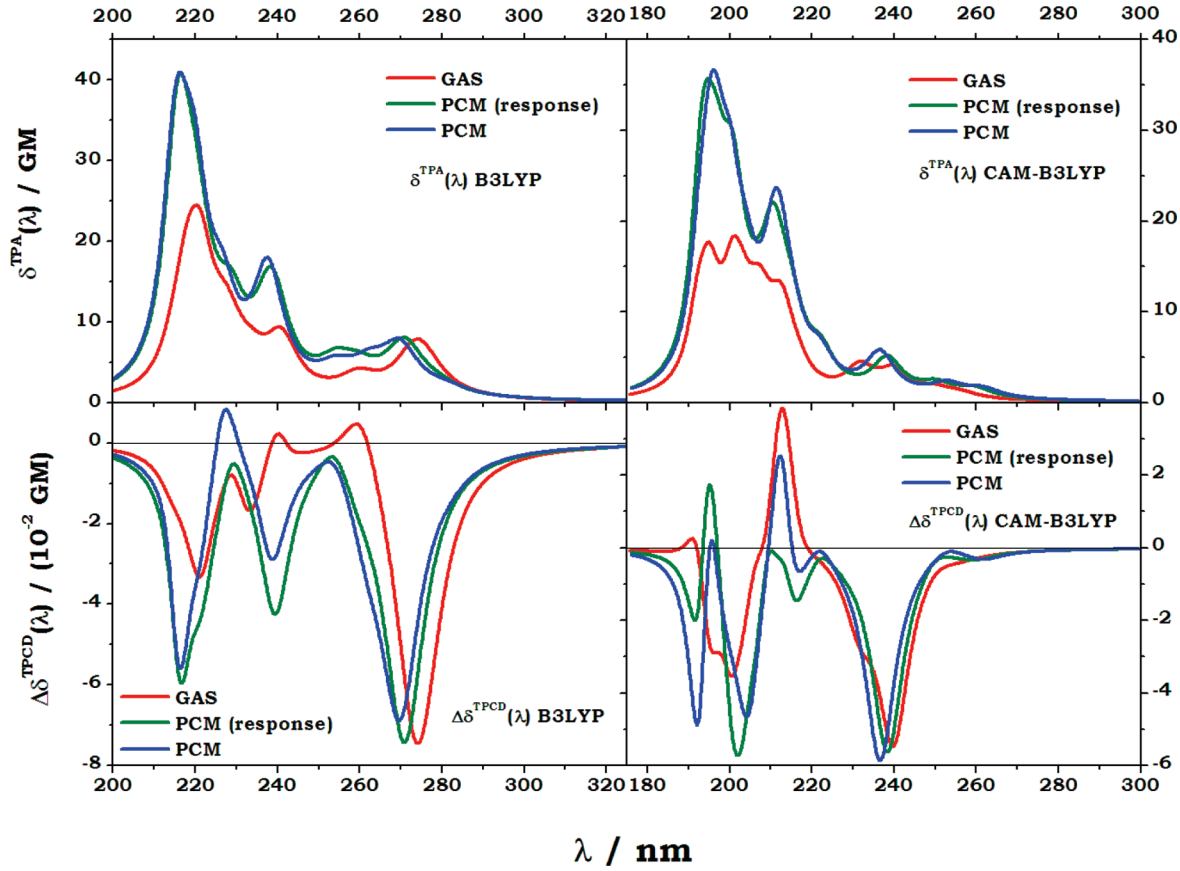

Figure 2. (L)-Tryptophan. TPA (top panels) and TPCD (bottom panels) spectra of the lowest conformer, originally conformer 1 in ref 48, simulated in the range where the 15 lowest excited electronic states obtained using the aug-cc-pVDZ basis set with both B3LYP (left panels) and CAM-B3LYP (right panels) are located. Results are obtained in the gas phase ("GAS") and in water, using the polarization continuum model either for response properties only ("PCM(response)") or for both structure relaxation and response properties ("PCM").

the 15 lowest excited electronic states are located in our computational analysis.

Analyzing the OPA spectra for both B3LYP and CAM-B3LYP, top panels in Figure 1, we observe that including the solvent in the simulation results in an increase in the absorbance and in a red shift of the absorption bands. In the case of CAM-B3LYP, the shape of the absorption bands is similar for the three calculations. For both B3LYP and CAM-B3LYP, the inclusion of PCM without accounting for the geometry relaxation yields for most of the band peaks placed between the gas and the solvent results. The intensity of the "PCM (response)" and "PCM" bands is also very similar and, as mentioned just above, larger than that seen for the gas phase. In the case of B3LYP, the differences between the gas phase and both solvent spectra are larger than for CAM-B3LYP. The band around 215 nm (gas/B3LYP) is shifted toward 220 nm in the solvent simulations. A similar effect occurs for the shoulder around 220 nm, for the weaker band placed around 230 nm, and for the peak at 275 nm (gas/B3LYP), shifting by ca. 5 nm with PCM. Also, the solvent shift appears to be slightly larger, reaching almost 10 nm, for B3LYP than for CAM-B3LYP.

As far as the comparison between the two functionals is concerned, Figure 1 shows that CAM-B3LYP yields spectra with significantly different shape with respect to B3LYP. It is well-known that the CAM-B3LYP excitation energies are systematically larger than those obtained with B3LYP, leading consistently to a blue shift of the spectra. Moreover, the splitting of the bands observed with the bandwidth selected for our analysis differs between the two methods. The two bands of different intensities, the one placed at 280 nm and the weaker one at 260 nm, observed in the left (B3LYP) panel get closer, forming a broad band roughly centered at about 260 nm on the right (CAM-B3LYP) panel. Also, where B3LYP predicts a single band at low wavelength (210 and 220 nm, in the gas phase and the solvent, respectively) accompanied by a small shoulder and a smaller band at slightly higher wavelength, CAM-B3LYP yields a broad absorption band, with four well-defined peaks, extending between 185 and 230 nm.

The adoption of a model for the solvent and the quality and features of the functional play a more important role for the ECD than for the OPA spectra (see the lower panels of Figure 1). A particularly significant effect is observed for example when the excitation energies and the ECD rotatory strengths are calculated with the PCM solvent model using nonrelaxed geometries. In this case the spectrum shows large deviations with respect to both the gas phase and the solvent (PCM) spectrum. While for OPA the differences were mainly related to the position of the bands, in this case also the relative intensities and the sign of the bands are affected. In the B3LYP ECD spectrum (bottom left panel), this difference appears mainly in the region between 210 and 230 nm. Outside this region, broadly speaking, the pattern is similar for the three cases. Only the intensity and the position of the dichroic bands vary, except at the highest wavelengths, between 250 and 290 nm. In that region the spectrum computed with PCM and relaxed geometries shows a very weak negative rotatory strength beyond 280 nm, whereas for the gas and the PCM nonrelaxed solvent cases, a broad band positive everywhere is observed. The relative position of the two last peaks differs also significantly between the gas phase, where they merge into a single peak centered

around 275 nm, and the two solvent cases, where they are split. The conclusion of the same analysis is slightly different for the CAM-B3LYP ECD spectrum. In this case, the two solvent spectra are rather similar—except possibly for the region between 215 and 220 nm, where a positive band appears in the nonrelaxed case, while the spectrum is negative for the full PCM case—and significantly different from the gas phase result. The differences mostly affect the sign of the spectrum in the lowest wavelength region, between 180 and 220 nm. In particular, in the region between 200 and 220 nm, the sign of the spectra is opposite in the gas phase compared to the solvent phase. It is also observed that the overall shape of the spectrum differs significantly between the two XC functionals. The integrated (absolute) rotatory strength is larger for CAMB3LYP than for B3LYP. The negative portion of the spectrum prevails, in both cases, especially for the PCM/CAM-B3LYP calculations. B3LYP predicts a pattern characterized by a positive band at the lowest wavelengths ($\lambda < 215$ nm), then a succession of negative peaks turning to positive around 235 nm and staying positive (except for the weak negative area discussed above beyond 280 nm in the PCM approximation) until ≈300 nm. The spectrum predicted with CAM-B3LYP has essentially a sequence of negative peaks between 180 and 220 nm (200 nm in the gas phase simulation), and it is almost everywhere positive beyond this region, with a strong dominant peak around 220 nm for the solvent cases and two bands (a double peak around 205 nm and a single peak just above 230 nm) in the gas phase calculation.

Since the geometries used for the CAM-B3LYP calculations are those obtained from the B3LYP geometry optimization, these differences are due only to the effect of the XC functional on the excited states and on the rotatory strengths. It is worth noting that CAM-B3LYP should in general only lead to significant improvements for long-range charge transfer excitations, and to some extent also for Rydberg excitations, whereas CAM-B3LYP excitation energies may in general be somewhat inferior to B3LYP for ordinary valence excitations.[78,79] Indeed, a recent study carried out on (*R*)-3-methyl-cyclopentanone,[25] similar to the present analysis on (L)-trp, reports significant differences in the excitation energies and in the position of the bands between B3LYP and CAM-B3LYP, with the latter being particularly effective in placing the one- and two-photon rotatory strength in the same wavelength range of experiment for the transitions to Rydberg-excited states. In contrast, B3LYP provides apparently a better agreement with experiment, with respect to CAM-B3LYP, in the simulation of the linear and nonlinear dichroism spectra of (*R*)-(+)-1,1′-bi(2-naphthol), where the response of valence-excited states is mainly probed (see refs 26 and 38). An improvement obtained with CAM-B3LYP in comparison to B3LYP in the determination of ECD rotational strength was proven using coupled-cluster and multireference CASSCF and RASSCF methods as reference calculations.[22,80] Despite this evidence, it is still important to go through an assessment of the functional to use, in our aim to propose a reliable scheme for the calculation of linear and nonlinear spectroscopic properties of a chiral system. This assessment will be completed, with a comparison with experiment, after a discussion of the effect of conformational averaging carried out in Section IV.B.

2. Two-Photon Processes. The TPA and TPCD spectra of the lowest conformer of (L)-trp are shown in the upper and lower panels, respectively, of Figure 2, for B3LYP (left panels) and CAM-B3LYP (right panels). Figure 2, as Figure 1, shows spectra obtained for the isolated gas phase molecule, for the PCM model associated with the gas phase geometry, and for the full solvent treatment. The reader should refer again to Table 1 in the Supporting Information for the detailed data on the B3LYP and CAM-B3LYP two-photon cross sections and two-photon rotatory strengths. The range of wavelengths in Figure 2, given as half the values employed in the two-photon experiment, is essentially that of Figure 1.

The inclusion of the solvent in the model yields systematically an increase of the TPA cross section, in particular for the most intense bands extending between 180 and 230 nm, regardless of the XC functional employed and of the structure. Relaxed and nonrelaxed geometries in PCM lead to almost the same spectra, with only small differences in the amplitude and the position of the bands. The analysis on this aspect is similar to the one done above for OPA, but in the case of TPA we observe an even smaller impact of geometry relaxation on the cross section. Adopting a nonrelaxed geometry leads already to a very good approximation of the spectrum computed with proper account of the electronic rearrangement occurring due to the PCM. Therefore, the dominant effect of a solvent model in TPA is on the transition properties, whereas in the one-photon case the two effects, geometry relaxation and the solvent effect on the electronic structure, are both of relevance. When comparing the TPA spectra simulated with the two different XC functionals, differences are mostly observed in the position and relative amplitude of the bands. The shift to lower wavelengths of the spectrum was discussed already for the linear spectroscopies. Concerning the shape of the bands, the most relevant differences are observed in the gas phase spectra for the broad band in the 180−220 nm range, where CAM-B3LYP predicts four peaks roughly of similar amplitude, collapsing to a structure made up by a dominant peak, a shoulder, and another weaker peak shifted to the 210−250 nm region with B3LYP.

The comparison of the spectra obtained for the different approximations is far less straightforward for TPCD. B3LYP yields a predominately negative TPCD spectrum. The two weak positive bands placed around 240 and 260 nm by B3LYP in the gas-phase calculations both disappear in the PCM(response) case, whereas a single positive dichroism is predicted by PCM around 230 nm. Two quite intense negative bands around 220 and 275 nm, respectively, are observed in the bottom left panel of Figure 2. The balance between positive and negative intensities is higher in the case of CAM-B3LYP, where the three curves in the bottom right panel of Figure 2 are very close to each other above 220 nm, with the intense negative band placed by B3LYP around 275 nm being blue-shifted by about 35 nm. Below 220 nm the two solvent approximations yield band shapes largely in reasonable agreement, although in this area there are quite a few states with rather sizable rotatory strengths of opposite sign (see Table 1 in the Supporting Information), and even small differences in the excitation energy lead to relevant changes in the band shapes with the choice of FWHM made. Therefore, both solvent calculations yield an alternation of negative and positive peaks, with a predominance of negative intensities and the positive peaks located at ≈195 nm in the PCM(response) case and at ≈215 nm in the PCM calculation. Below 210 nm, the gas-phase spectrum displays a somewhat simpler pattern, with a broad two-peaked negative band around 200 nm and a positive peak placed at ≈215 nm.

The two XC functionals yield approximately the same integrated absolute TPCD rotatory strength in the range of wavelengths of our study. The corresponding integrated TPA intensity is sizeably larger (10−25%, depending on the approximation) when computed with B3LYP with respect to

CAM-B3LYP. This behavior opposes that seen for the linear spectroscopies where both OPA and ECD increase their integrated (absolute) intensities by as much as 50−60% when going from B3LYP to CAM-B3LYP. Besides intensities, it is apparent from what we have seen above that the form and the shape and location of the bands depend heavily on the choice of functional. Limiting the analysis to B3LYP and CAM-B3LYP, the two XC functionals employed in our study, it is clear that the origin of the differences is the energetic reordering of the excited states occurring when the long-range correction is introduced with CAM-B3LYP.

B. Effects of Conformational Averaging. The first part of the present study has shown that the influence of the solvent leads in some instances to large changes in the simulated spectra, in terms of not only the position but also the relative amplitude of the absorption and dichroic bands. This observation is of major importance to develop a predictive tool to be employed in comparison with experimental spectra. We have also observed that the geometry relaxation in the solvent plays a role which is less important than the effect of the environment on the electronic properties. Last, but not least, the choice of the functional in the time-dependent DFT calculations is a far from trivial and easily rationalized task. Nevertheless, some guidelines can probably be given and some rules of thumbs established, if it is made sufficiently clear that they should be used with extreme care. There is evidence that a polarizable continuum model introduced to account for the effect of the environment might be quite effective for the description of absorption processes in the condensed phase, yielding in cases some decisive improvements over isolated molecule models in reproducing features seen in experiment even for nonlinear circular dichroism spectra (see for instance ref 26). Therefore, as condensed-phase models are nowadays available at a reasonable cost for the simulation of linear and nonlinear spectroscopic properties, the advice is that they should be used when dealing with processes in which the environment is expected to play a role. PCM, in spite of some shortcomings arising when dealing with specific interactions in solution or in pure liquids, appears to be in several cases rather efficient in catching the most important effects of the intermolecular interactions in the condensed phase, at least for the spectroscopies studied here. The discussion of the "optimal" choice of the functional in TDDFT studies of linear and—even more importantly—nonlinear spectroscopic properties is bound to be very complex, mainly due to the plethora of functionals available on the market. If we restrict the field to B3LYP and to the standard formulation of CAM-B3LYP, the two functionals employed here, it is perhaps possible to state that the latter can be quite effective in reproducing at least the position of the bands involving Rydberg transitions or transitions involving diffuse orbitals (see, for instance, refs 25, 27, and 44), whereas in some cases B3LYP is somewhat superior for valence excitations.[26] Nevertheless, to go further in the development of a reliable and general methodology for the simulation of linear and nonlinear absorption or dichroism spectroscopies, there is another aspect that needs to be considered for flexible molecular systems: the existence in the sample of different, energetically close-lying conformers, whose response can be quite different, and which may be differently populated at finite temperatures.

In this section we analyze the consequences of performing a Maxwell−Boltzmann (MB) conformational averaging on the spectra simulated for the OPA, ECD, TPA, and TPCD spectra of the lowest conformers of (L)-trp in the gas phase and in water solution. This allows us to simulate the effect of a finite temperature on the spectra. The MB weights, obtained as described in Section III, are given in Table 1 for a temperature of 298.15 K and a pressure of 1 atm. The conformers are given numerical labels, according MB weights, both in the gas phase and in water. The correspondence between the current labels for the gas phase conformers and those assigned by Huang and Lin in ref 48 is given in parentheses in Table 1. There is no systematic link between conformers having the same label in the gas phase and in water. The number of most stable conformers initially selected in our study was ten and eleven, in the gas phase and in water, respectively. Of the eleven zwitterionic structures, only nine are kept in our analysis since the MB weight of the tenth and eleventh were found to be negligible (less than 0.1% of the population at 298.15 K). Note that the same MB weight is used for a given conformer in both the B3LYP and CAM/B3LYP calculation of the spectroscopic properties.

In the gas phase, the most populated conformer contributes to 39.1% of the total average. The two next conformations are attributed to 15.4% and 14.7%, respectively, of the total population, with the remaining seven structures contributing in percentages ranging from 8.6 to 2.7%. In the solvent phase, the situation is slightly different: the four lowest conformations contribute all significantly to the spectrum, with MB weights of 37.8, 31.5, 11.2, and 10.2, respectively. The Boltzmann averaged spectra are therefore in both cases the result of the mixing of the features of different conformers. This is more evident to some extent in the water calculations, making in this case conformational averaging an especially mandatory step and the spectral features in some cases richer than those observed for the isolated molecule.

1. One-Photon Processes. Let us focus first on the OPA and the ECD spectra of (L)-trp. In Figures 3 and 4, the OPA and ECD spectra of the lowest, most populated conformers of (L)-trp in the gas phase (neutral, left panels) and in water solution (zwitterions, right panels), respectively, are shown. Again, the range of wavelengths of the spectra encompasses the region where the 15 lowest excited states of each conformer are located, covering the interval between 180 and 300 nm. As for the first part of the study, the oscillator strengths f_{0n} and the rotatory strengths ${}^{n}R$ are given, for each conformer, in the Supporting Information (see Tables II−V therein).

In each panel, the thick dark curve represents the MB weighted spectra obtained from the individual conformers. At a given wavelength, the algebraic sum of the individual (thin, in color) spectra yields the value of the MB averaged (thick dark) line; i.e., the individual spectra shown are already multiplied by the MB weights, given for convenience for each conformer in the legends (see also Table 1).

As noted already in Section IV.A, the results vary significantly from one computational level to the other. In the gas phase, the OPA B3LYP spectrum is dominated by the contribution of the first conformer, whose spectrum is therefore very close to that corresponding to the MB average. A strong band is centered around 215 nm, characterized in its broad high wavelength end which extends to about 250 nm by a sequence of shoulders. Two significant peaks are centered a bit below 260 nm and around 275 nm, respectively. In the gas phase/CAM-B3LYP OPA spectrum the intense band at low wavelengths extends from 180 to beyond 220 nm, and it is structured, with two peaks of different intensities and a shoulder, partially reproducing the features of the lowest conformer especially as far as the multiplicity and position of the peaks are concerned. Indeed, between 200 and 210 nm, all the remaining conformers display

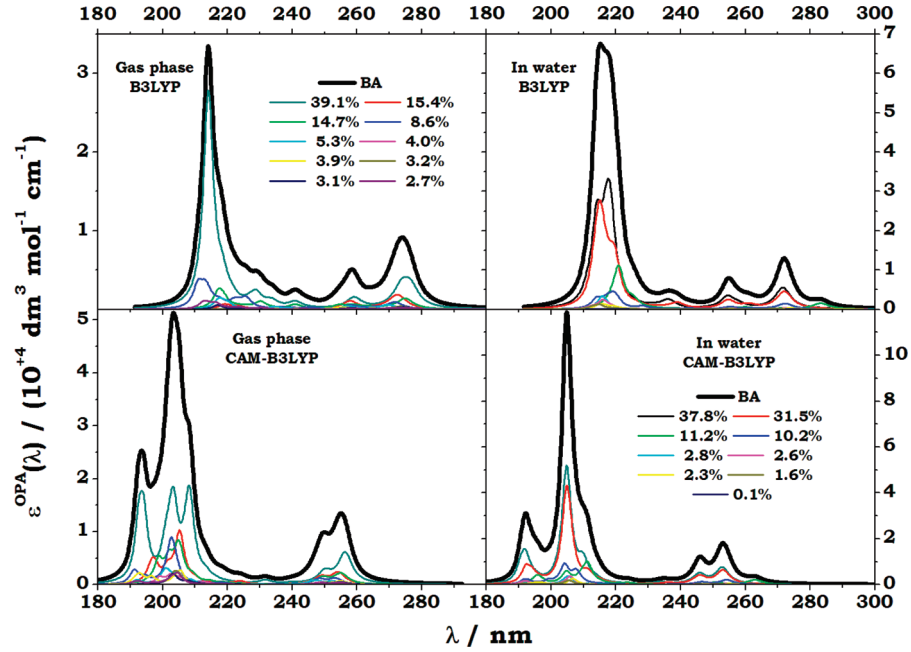

Figure 3. (L)-Tryptophan. OPA spectra of the 10 lowest neutral conformers in the gas phase (left panels) and the 9 lowest zwitterionic conformers in water (right panels), respectively, in the range where the 15 lowest excited electronic states are obtained using the aug-cc-pVDZ basis set with B3LYP (top panels) and CAM-B3LYP (bottom panels). The legend gives the Boltzmann weight of each conformer. The thick, dark curves represent the Boltzmann averaged spectra.

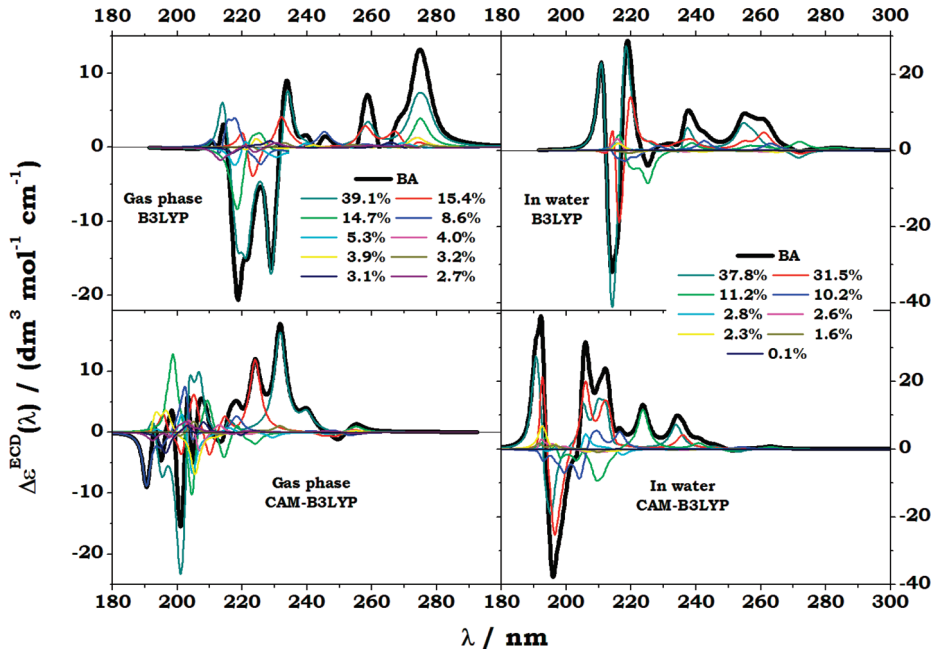

Figure 4. (L)-Tryptophan. ECD spectra of the 10 lowest neutral conformers in the gas phase (left panels) and the 9 lowest zwitterionic conformers in water (right panels), respectively, in the range where the 15 lowest excited electronic states are obtained using the aug-cc-pVDZ basis set with B3LYP (top panels) and CAM-B3LYP (bottom panels).The legend gives the Boltzmann weight of each conformer. The thick, dark curves represent the Boltzmann averaged spectra.

strong absorption bands, enhancing then the intensity of the middle peak of the MB averaged spectrum. We have already seen and discussed in the previous section how the choice of the XC functional influences the spectroscopic response of the first gas-phase conformer, which is indeed the structure on which the analysis of Section IV.A is based.

Turning to the B3LYP OPA spectrum in water, it can be seen that the peak at 215 nm in the gas phase stays in the same area. It is a bit more intense, and it broadens slightly since the two lower zwitterionic conformers, contributing by roughly 40% and 30% to the average, have a maxima of absorption slightly displaced and split in two peaks with asymmetric and opposite intensity in the two structures. The peaks seen at ≈260 and 275 nm in gas appear also in water. Note a weak absorption appearing at 280 nm, due almost entirely to the third zwitterionic conformer (ca. 11% of the population). The broad structured band seen in the gas/CAM-B3LYP simulation between 180 and 220 nm is heavily modified when the effect of the environment is included in the water/CAM-B3LYP calculations. The central peak becomes twice as intense, turning the peak on the red side into a shoulder (receiving intensity as expected from both the first and second conformer but also, somewhat surprisingly, by

the third conformer, whose most intense band is due to the eight excited state at 211.1 nm; see Table 5 in Supporting Information) and borrowing some intensity from the one on the blue side. The band between 240 and 265 nm remains largely unchanged.

The discussion of the ECD spectra shown in Figure 4 is far from trivial, and we limit ourselves here to a discussion of the general features. With the exception to some extent of the gas/CAM-B3LYP spectrum, broadly speaking the Boltzmann averaged ECD spectrum of (L)-trp in the 180−300 nm range is a sequence of a positive peak (at ≈210 nm according to B3LYP, more like ≈190 nm if we decide to trust CAM-B3LYP), then a negative peak, 15 nm wide in the gas/B3LYP calculation, reduced to 5−10 nm in both the water calculations, then an area of predominantly positive bands extending to the upper end of the interval. In the gas/CAM-B3LYP calculation, the initial positive peak is missing, the reason being the strong negative rotatory strength (-8.93×10^{-5} au) of state 15 (the last of the set) for conformer 4 (see Table 3 in the Supporting Information). This is therefore a frontier state, and since the choice of the number of excited states to be included in the analysis (15 in this work) is somewhat arbitrary, as it is dictated roughly by the need to balance computational cost and accuracy in the response calculations, the presence or absence of the positive peak at the lower end of our wavelength interval is of relatively little relevance. The general features of the ECD spectra just outlined hide in Figure 4 a large number of details that have a complex dependence on all parameters of the calculations. In particular, the wide range of responses of the individual conformers is a striking feature of Figure 4. As already noted, a detailed analysis is of little use, also in view of the fact that the sequence of well-resolved peaks is a consequence of the relatively small value chosen for the FWHM. We also note the usual shift, by 15−20 nm, toward the blue of the spectral features of CAM-B3LYP vs B3LYP.

To try to shed some light on the reliability of our analysis, we can compare our conformational averaged OPA and ECD spectra, obtained in water, with experimental results. The far-UV experimental OPA and ECD spectra of (L)-trp were recorded and reported by Auer in 1973.[76] Our results (both B3LYP and CAM-B3LYP) and experiment are shown in Figure 5, the ECD in the top panel and the OPA at the bottom. The experimental range of frequency goes from 180 to 250 nm. The resolution of the experimental spectrum, as can be deduced from the data drawn by Auer, corresponds roughly to a FWHM of 15−20 nm, which, in the range of wavelengths of the spectrum, translates into ≈0.35 −0.65 eV. For this reason we superimpose in Figure 5 spectra simulated both with a FWHM of 0.1 eV (dotted thin curves, FWHM taking values between 3 and 4 nm in the region of the spectrum) and 0.3 eV (solid thick curves, FWHM between 9 and 12 nm in the same range). Simulated spectra have been scaled in intensity by multiplying the computed data by a factor of 3. This was done so that the experimental and (broader) simulated spectra could have comparable intensities. Note that the units used in the experiment were the relative absorbance for the one-photon absorption and the molar ellipticity for the ECD. The units on the vertical axes of Figure 5 are therefore arbitrary. The thick curves provide the best comparison with experiment, whereas the thin dotted profiles provide a better insight on the complexity of the response.

The experimental OPA spectrum shows two maxima, a narrower, more intense one located a bit below 220 nm and a broader weaker one centered roughly around 190 nm. This pattern is well reproduced by our PCM/CAM-B3LYP, also with

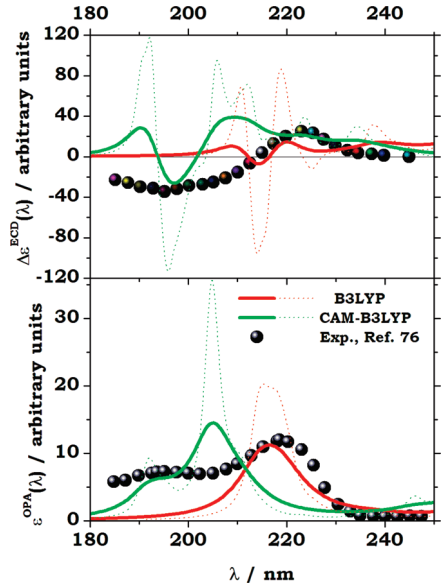

Figure 5. (L)-Tryptophan. OPA and ECD spectra, simulated via a Boltzmann average over the response of the 9 lowest zwitterionic conformers in water (top panel)—both B3LYP and CAM-B3LYP results—compared with the experimental spectra taken from ref 76.

a reasonable relative ratio of intensities for the two maxima. The position of the peak on the blue side is well reproduced, whereas that on the red side appears to be blue-shifted by about 15 nm (205 nm in PCM/CAM-B3LYP). A peak appears at about 245 nm, at the upper edge of the experiment, and it is appreciated essentially only when a FWHM of 0.1 eV is employed in the simulation. PCM/B3LYP yields a single band (with two close lying peaks) at 215 nm that is very close to the position of the second peak of experiment. Note that the simulations using different values of the FWHM yield in both CAM-B3LYP and B3LYP essentially the same patterns. As far as the ECD spectrum is concerned, experiment sees a broad positive band between 210 and 245 nm, followed by a broad negative band extending between 180 and 210 nm. As already discussed previously in this section, our PCM/B3LYP simulation of (L)-trp in water yields (Figure 5) a positive band extending above 215 nm, with a (narrower) peak at about 220 nm and wide plateau around 235−240 nm, followed by a negative area only 5 nm wide, between 210 and 215 nm, and then the signal goes back to positive between 210 and 180 nm. The use of a FWHM of 0.3 eV hides the negative band between ≈225 and 230 nm discernible with the choice of a smaller bandwidth. The simulation carried out at the PCM/CAM-B3LYP level has the same features, roughly shifted toward lower wavelengths by approximately 15 nm. Roughly speaking, as for the OPA spectrum, B3LYP is closer to experiment as far as the position of the maximum of the high-wavelength positive band is concerned (≈220 −225 nm), whereas CAM-B3LYP fares better compared to B3LYP with respect to the position of the (absolute) maximum of the negative band at lower wavelength (≈195 nm). The change in sign apparently predicted by theory at higher energies is, as already discussed above, to be taken with care, as the effect of the strong positive rotatory strength of the frontier excited states responsible for the positive peak in that region might well be canceled by near-lying higher excited states not included in our analysis. Note that a further increase of the FWHM in our simulation of the ECD spectra in water (for instance, the use of values of FWHM of 0.5−0.6

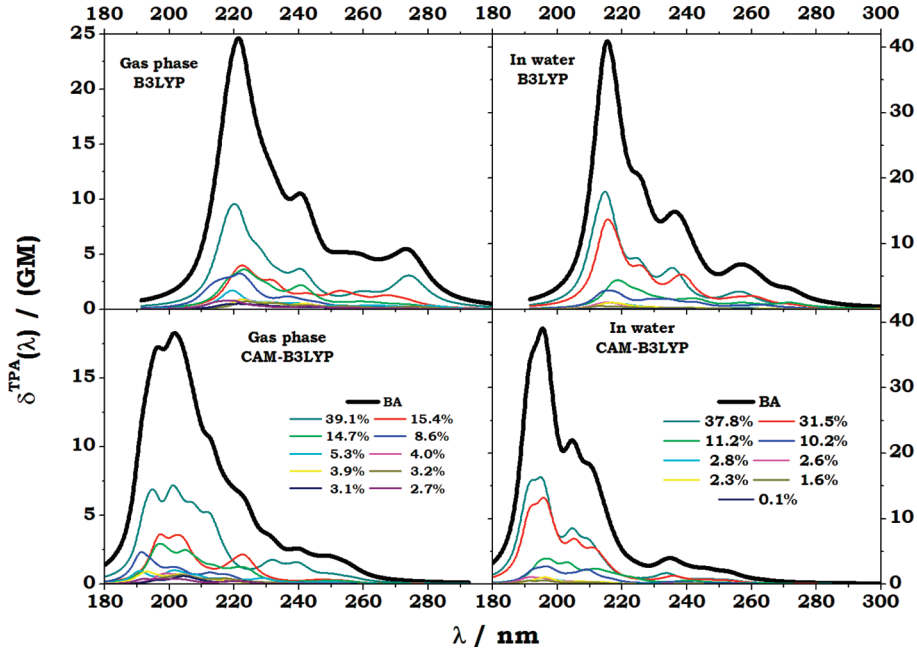

Figure 6. (L)-Tryptophan. TPA spectra of the 10 lowest neutral conformers in the gas phase (left panels) and the 9 lowest zwitterionic conformers in water (right panels), respectively, in the range where the 15 lowest excited electronic states are obtained using the aug-cc-pVDZ basis set with B3LYP (top panels) and CAM-B3LYP (bottom panels). The legend gives the Boltzmann weight of each conformer. The thick, dark curves represent the Boltzmann averaged spectra.

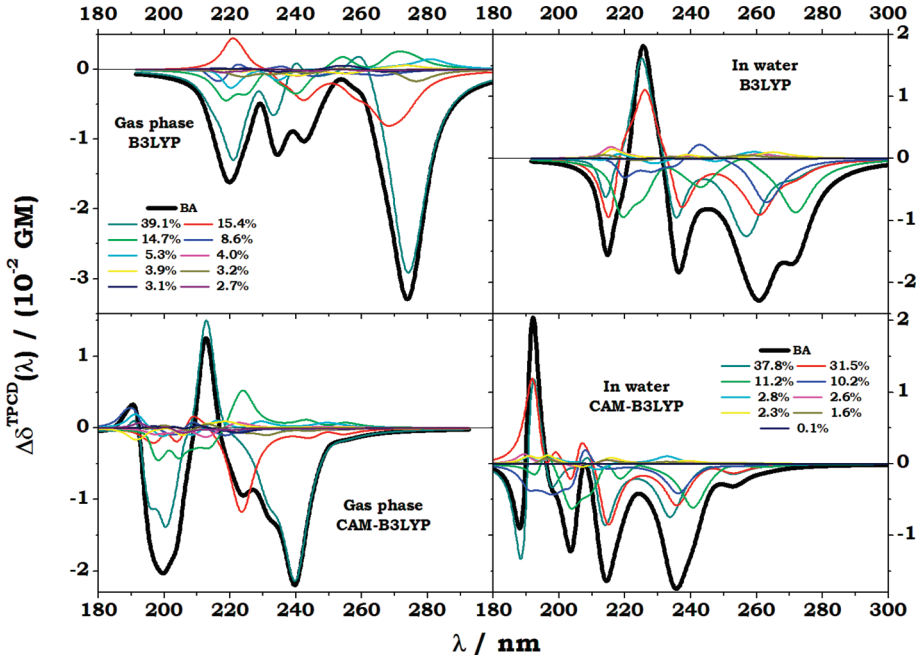

Figure 7. (L)-Tryptophan. TPCD spectra of the 10 lowest neutral conformers in the gas phase (left panels) and the 9 lowest zwitterionic conformers in water (right panels), respectively, in the range where the 15 lowest excited electronic states are obtained using the aug-cc-pVDZ basis set with B3LYP (top panels) and CAM-B3LYP (bottom panels). The legend gives the Boltzmann weight of each conformer. The thick, dark curves represent the Boltzmann averaged spectra.

eV) has the effect of canceling completely the negative band seen in the simulated ECD spectra both with B3LYP and CAM-B3LYP.

2. Two-Photon Processes. Figure 6 and Figure 7 show the four TPA and TPCD spectra, respectively, of the most stable conformers in the gas phase (left panels) and in water (right panels), obtained as for the one-photon processes discussed above, for the B3LYP (top panels) and CAM-B3LYP (bottom panels) XC functionals. For the TPA spectra, the conclusions that can be drawn are similar to those reported above for OPA. The first conformer dictates the form of the spectra in the gas phase calculations. In water, both the first and second conformers are contributing sizeably, and their spectra are quite similar, for B3LYP as well as for CAM-B3LYP. Besides the general blue shift, by 15−20 nm, observed with CAM-B3LYP with respect to B3LYP, a feature arising from the comparison of the two XC functionals is the large deviation in the relative intensity and in the position of the absorption bands of the individual conformers, highlighting a significant reshuffling of the excitation energies and nonlinear responses of the 15 lower-lying excited states obtained by the two methods. This variety is observed both in the gas phase and in water.

Figure 7 shows that the different parameters of our calculations play a very important role in the simulation of the TPCD spectra. B3LYP predicts in the gas phase a sequence of negative bands throughout the whole range of the spectrum. This behavior is unique among the four panels in Figure 7, since in all other simulations an intense positive peak appears at wavelengths varying from 190 nm (water/CAM-B3LYP) to 210 nm (gas/CAM-B3LYP) to 225 nm (water/B3LYP). Some insight into this phenomenon is given by an analysis of the rotatory strengths in the tables collected in the Supporting Information. The state mostly responsible for the positive peak seen in both water/B3LYP and gas/CAM-B3LYP calculations is the seventh, yielding TPCD rotatory strengths ${}^fR^{TP}$ ranging from +400 to +600 au for the conformers contributing to the MB average in the two spectra. The displacement of the peaks (ca. 20 nm) is accounted for as usual by the blue shift noted in this region for CAM-B3LYP with respect to B3LYP. The seventh excited state has a negative (and sizable, ca. −180 au) TPCD rotatory strength in the gas/B3LYP calculation of the lowest conformer, where it sits only 6−7 nm away from state number six, displaying a ${}^fR^{TP} \approx +300$ au, and ca. 8 nm from state five, ${}^fR^{TP} \approx -190$ au. In this area the combined strengths yield a weak positive absorption, in a narrow range (around 240 nm) where conformers two and three display notable negative TPCD peaks. As a result, around 240 nm the TPCD has a negative minimum (in absolute terms) occurring between the two higher lying (negative) peaks of the broad band placed between 190 and 255 nm. Finally, in the water/CAM-B3LYP simulation the strong TPCD rotatory strength responsible for the positive peaks in the gas/CAM-B3LYP and water/B3LYP spectra is attributed for the lowest conformer to state number twelve ($\lambda = 191.8$ nm, ${}^fR^{TP} \approx +590$ au), with the close-by thirteenth state ($\lambda = 190.7$ nm) also displaying a sizable positive response (${}^fR^{TP} \approx +180$ au) and state number fourteen ($\lambda = 189.8$ nm) with a large negative ${}^fR^{TP}$ (≈−490 au). In the second conformer, contributing to the MB average only slightly less than the first, the positive rotatory strength is distributed between excited states twelve and fourteen, located between 192 and 194 nm. Therefore, the shift in the position of the positive peak with respect to the gas/CAM-B3LYP case is due to the redistribution of the rotatory strengths due to the solvent effect. The high wavelength area of all spectra in Figure 7 is negative, regardless of the approximation. Note that the overall structure of the TPCD spectrum (L)-trp mirrors that of the corresponding ECD profile, especially in water, with the latter displaying a predominantly positive dichroism and a somewhat isolated negative peak, essentially the opposite of what is predicted for the nonlinear dichroism.

V. Summary and Outlook

We have presented a detailed study of the computational requirements needed for the calculation of linear and nonlinear chiroptical properties of the model amino acid (L)-tryptophan, in an attempt to set an accurate and reliable protocol for the prediction of spectra of molecules of biological interest. The effects of the choice of XC functional, restricted here to B3LYP and CAM-B3LYP, were investigated, as were the effects of the solvent, described in this work by the PCM. Both the direct effects of PCM on the electronic response properties, as well as the indirect effects due to changes in the molecular structures induced by the dielectric medium, were studied. Finally, the effects of the different contributing conformations on the simulated OPA, ECD, TPA, and TPCD spectra were analyzed, and a comparison with experimental spectra was carried out for the one-photon spectra.

The adoption of B3LYP and CAM-B3LYP XC functionals leads in many cases to qualitatively and quantitatively different spectra for both the linear and nonlinear properties.

The effect of relaxing the geometry varies for the different properties and with the choice of XC functional. It appears also mandatory to employ solvent-optimized structures, especially for fairly polar molecules such as (L)-trp, to properly describe the influence of the surrounding solvent molecules. Although the effects may in some cases be negligible, our study has demonstrated that they cannot however be neglected a priori.

A very important step in the simulation of one- and two-photon spectra in the case of flexible molecules such as (L)-trp is the conformational averaging. The importance of a proper conformational search is clearly demonstrated in the case of chiroptical properties such as ECD and TPCD. This is in agreement with earlier observations for ECD,[81,82] and the evidence is extended here also to the two-photon analogue. Upon solvation, the relative stability of the different conformers and their geometry can change dramatically. Since different conformations can have quite different chiroptical spectra, the introduction of a solvent model may yield ECD and TPCD spectra that have very little in common with those obtained in the gas phase.

Earlier studies have demonstrated the superiority and robustness of CAM-B3LYP for excited-state properties and excitation energies of molecules.[19−22] On our side, we have seen cases where CAM-B3LYP, in its standard formulation, was particularly effective in studies of one- and two-photon spectroscopies of solvated *R*-(+)-3-methyl-cyclopentanone,[25,27,44,45] in particular where excitations to diffuse Rydberg-type orbitals were involved, whereas little benefit if any was seen in studies of linear and nonlinear one- and two-photon spectroscopies of (*R*)-(+)-1,1′-bi(naphthol),[26,38] where the most important features of the spectrum involved valence excitations. In the present study, the comparison of our simulated OPA and ECD spectra in water solution with experimental data shows that the major features, i.e., the profile of the spectra, are reasonably well described by both B3LYP and CAM-B3LYP and that the latter reproduces the position of the experimental peaks better than the former in the high-energy region (where excitations are more diffuse), whereas the reverse occurs in the low-energy region, where the excited states have a valence-like character.

Our study has thus demonstrated the importance of the choice of XC functional, of the choice of reference geometries, and of the inclusion of solvent effects.

It is possible to argue that the task we decided to undertake with this study is quite complex and ambitious, and there are so many shortcomings and approximations in our approach that an attempt to establish a foolproof protocol for the prediction of linear and nonlinear absorption and dichroism spectra of complex biological systems in their native environment might easily be considered rather hopeless with today's computational tools. Furthermore, (L)-tryptophan is just one of the proteinogenic amino acids, and the transferability of any conclusion to other amino acids or biological system would need to be carefully addressed. However, agreement between theory and experiment is reasonably good, lending support to the models used.

Despite possible shortcomings in the detailed description of the solvation process, we believe that the present work represents an important step toward the understanding of computational requirements for the study of (multi)photon chiroptical properties of biologically important molecules in their native environment.

Acknowledgment. This work has received support from the Norwegian Research Council through a Centre of Excellence

Grant (Grant No 179568/V30), an YFF grant to KR (Grant No 162746/V00), as well as through a grant of computer time from the Norwegian Supercomputing Program.

Supporting Information Available: Tables I−V. This material is available free of charge via the Internet at http://pubs.acs.org.

References and Notes

(1) Condon, E. U. *Rev. Mod. Phys.* **1937**, *55*, 2789.
(2) Craig, D. P.; Thirunamachandran, T. *Molecular Quantum Electrodynamics. An Introduction to Radiation Molecule Interaction*; Dover Publications, Inc.: Mineaol, NY, 1984.
(3) Barron, L. D. *Molecular light scattering and optical activity*; Cambridge University Press: Cambridge, 2004.
(4) Nafie, L. A.; Keiderling, T. A.; Stephens, P. J. *J. Am. Chem. Soc.* **1976**, *98*, 2715.
(5) Hecht, L.; Barron, L. D. In *Modern aspects Of Raman Spectroscopy*; Laserna, J. J., Ed.; Wiley: New York, 1996; pp 265−304.
(6) Göppert-Mayer, M. *Ann. Phys. (Leipzig)* **1931**, *9*, 273.
(7) Lin, S. H.; Fujimura, Y.; Neusser, H. J.; Schlag, E. W. *Multiphoton Spectroscopy of Molecules*; Academic Press: New York, 1984.
(8) Lambropoulos, P. Eberly, J. H., Eds. *Multiphoton Processes*; Wiley Interscience: New York, 1978.
(9) Tinoco, I., Jr. *J. Chem. Phys.* **1975**, *62*, 1006.
(10) Olsen, J.; Jørgensen, P. *J. Chem. Phys.* **1985**, *82*, 3235.
(11) Olsen, J.; Jørgensen, P. In *Modern Electronic Structure Theory, Part II*; Yarkony, D. R., Ed.; World Scientific: Singapore, 1995; p 857.
(12) Sałek, P.; Vahtras, O.; Helgaker, T.; Ågren, H. *J. Chem. Phys.* **2002**, *117*, 9630.
(13) Jansík, B.; Rizzo, A.; Ågren, H. *Chem. Phys. Lett.* **2005**, *414*, 461.
(14) Rizzo, A.; Jansík, B.; Bondo Pedersen, T.; Ågren, H. *J. Chem. Phys.* **2006**, *125*, 064113.
(15) Becke, A. D. *J. Chem. Phys.* **1993**, *98*, 5648.
(16) Becke, A. D. *Phys. Rev. A* **1988**, *38*, 3098.
(17) Lee, C.; Yang, W.; Parr, R. G. *Phys. Rev. B* **1988**, *37*, 785.
(18) Stephens, P. J.; Devlin, F. J.; Chabalowski, C. F.; Frisch, M. J. *J. Phys. Chem.* **1994**, *98*, 11623.
(19) Yanai, Y.; Tew, D. P.; Handy, N. C. *Chem. Phys. Lett.* **2004**, *393*, 51.
(20) Peach, M. J. G.; Helgaker, T.; Sałek, P.; Keal, T. W.; Lutnæs, O. B.; Tozer, D. J.; Handy, N. C. *Phys. Chem. Chem. Phys.* **2006**, *8*, 558.
(21) Paterson, M. J.; Christiansen, O.; Pawłowski, F.; Jørgensen, P.; Hättig, C.; Helgaker, T.; Sałek, P. *J. Chem. Phys.* **2006**, *124*, 054322.
(22) Shcherbin, D.; Ruud, K. *Chem. Phys.* **2008**, *349*, 234.
(23) Jansík, B.; Rizzo, A.; Ågren, H. *J. Phys. Chem. B* **2007**, *111*, 446. Erratum, ibid **2007** *111*, 2409.
(24) Jansík, B.; Rizzo, A.; Ågren, H.; Champagne, B. *J. Chem. Theor. Comput.* **2008**, *4*, 457.
(25) Rizzo, A.; Lin, N.; Ruud, K. *J. Chem. Phys.* **2008**, *128*, 164312.
(26) Toro, C.; De Boni, L.; Lin, N.; Santoro, F.; Rizzo, A.; Hernández, F. E. *Chem.−Eur. J.* **2010**, *16*, 3504.
(27) Lin, N.; Santoro, F.; Rizzo, A.; Luo, Y.; Zhao, X.; Barone, V. *J. Phys. Chem. A* **2009**, *113*, 4198.
(28) Szłucki, J.; Stręk, W. *J. Chem. Phys.* **1986**, *85*, 5547.
(29) Gunde, K. E.; Richardson, F. S. *Chem. Phys.* **1995**, *194*, 195.
(30) Hache, F.; Mesnil, H.; Schanne-Klein, M. C. *Phys. Rev. B* **1999**, *60*, 6405.
(31) Mesnil, H.; Hache, F. *Phys. Rev. Lett.* **2000**, *85*, 4257.
(32) Mesnil, H.; Schanne-Klein, M. C.; Hache, F.; Alexandre, M.; Lemercier, G.; Andraud, C. *Chem. Phys. Lett.* **2001**, *338*, 269.
(33) Mesnil, H.; Schanne-Klein, M. C.; Hache, F. *Phys. Rev. A* **2002**, *66*, 013802.
(34) Alexandre, M.; Lemercier, G.; Andraud, C.; Mesnil, H.; Schanne-Klein, M. C.; Hache, F. *Synth. Met.* **2002**, *127*, 135.
(35) Markowicz, P. P.; Samoc, M.; Cerne, J.; Prasad, P. N.; Pucci, A.; Ruggeri, G. *Opt. Express* **2004**, *12*, 5209.
(36) De Boni, L.; Toro, C.; Hernández, F. E. *Opt. Lett.* **2008**, *33*, 2958.
(37) Wanapun, D.; Wampler, R. D.; Begue, N. J.; Simpson, G. J. *Chem. Phys. Lett.* **2008**, *455*, 6.
(38) Toro, C.; De Boni, L.; Lin, N.; Santoro, F.; Rizzo, A.; Hernández, F. E. *Chirality*, in press.
(39) Miertuš, S.; Scrocco, E.; Tomasi, J. *Chem. Phys.* **1981**, *55*, 117.
(40) Cammi, R.; Tomasi, J. *J. Comput. Chem.* **1995**, *16*, 1449.
(41) Tomasi, J.; Mennucci, B.; Cammi, R. *Chem. Rev.* **2005**, *105*, 2999.
(42) Kierdaszuk, B.; Gryczynski, I.; Modrak-Wojcik, A.; Bzowska, A.; Shugar, D.; Lakowicz, J. R. *Photochem. Photobiol.* **1995**, *61*, 319.
(43) Blom, M. N.; Compagnon, I.; Polfer, N. C.; von Helden, G.; Meijer, G.; Suhai, S.; Paizs, B.; Oomens, J. *J. Phys. Chem. A* **2007**, *111*, 7309.
(44) Lin, N.; Luo, Y.; Santoro, F.; Zhao, X.; Rizzo, A. *Chem. Phys. Lett.* **2008**, *464*, 144.
(45) Lin, N.; Santoro, F.; Zhao, X.; Rizzo, A.; Barone, V. *J. Phys. Chem. A* **2008**, *112*, 12401.
(46) McClain, W. M. *Acc. Chem. Res.* **1974**, *7*, 129.
(47) Bondo Pedersen, T.; Koch, H.; Ruud, K. *J. Chem. Phys.* **1999**, *110*, 2883.
(48) Huang, Z.; Lin, Z. *J. Phys. Chem. A* **2005**, *109*, 2656.
(49) Klamt, A.; Schüürmann, G. *J. Chem. Soc., Perkin Trans.* **1993**, *2*, 799.
(50) Andzelm, J.; Kölmel, C.; Klamt, A. *J. Chem. Phys.* **1995**, *103*, 9312.
(51) Barone, V.; Cossi, M. *J. Phys. Chem. A* **1998**, *102*, 1995.
(52) Cossi, M.; Rega, N.; Scalmani, G.; Barone, V. *J. Comput. Chem.* **2003**, *24*, 669.
(53) Takano, Y.; Houk, K. N. *J. Chem. Theory Comput.* **2005**, *1*, 70.
(54) Dunning, T. H., Jr. *J. Chem. Phys.* **1989**, *90*, 1007.
(55) Mikkelsen, K. V.; Cesar, A.; Ågren, H.; Jensen, H. J. A. *J. Chem. Phys.* **1995**, *103*, 9010.
(56) Cammi, R.; Frediani, L.; Mennucci, B.; Tomasi, J.; Ruud, K.; Mikkelsen, K. V. *J. Chem. Phys.* **2002**, *117*, 13.
(57) Cammi, R.; Frediani, L.; Mennucci, B.; Ruud, K. *J. Chem. Phys.* **2003**, *119*, 5818.
(58) Kongsted, J.; Bondo Pedersen, T.; Osted, A.; Hansen, A. E.; Mikkelsen, K. V.; Christiansen, O. *J. Phys. Chem. A* **2004**, *108*, 3632.
(59) Pecul, M.; Marchesan, D.; Ruud, K.; Coriani, S. *J. Chem. Phys.* **2005**, *122*, 024106.
(60) Frediani, L.; Rinkevicius, Z.; Ågren, H. *J. Chem. Phys.* **2005**, *122*, 244104.
(61) Zhao, K.; Ferrighi, L.; Frediani, L.; Wang, C.-K.; Luo, Y. *J. Chem. Phys.* **2007**, *126*, 204509.
(62) Ferrighi, L.; Frediani, L.; Fossgaard, E.; Ruud, K. *J. Chem. Phys.* **2007**, *127*, 244103.
(63) Cappelli, C.; Mennucci, B.; Tomasi, J.; Cammi, R.; Rizzo, A.; Rikken, G. L. J. A.; Mathevet, R.; Rizzo, C. *J. Chem. Phys.* **2003**, *118*, 10712.
(64) Cappelli, C.; Mennucci, B.; Cammi, R.; Rizzo, A. *J. Phys. Chem. B* **2005**, *109*, 18706.
(65) Jansík, B.; Rizzo, A.; Frediani, L.; Ruud, K.; Coriani, S. *J. Chem. Phys.* **2006**, *125*, 234105.
(66) Rizzo, A.; Frediani, L.; Ruud, K. *J. Chem. Phys.* **2007**, *127*, 164321.
(67) Rizzo, A. In *Continuum solvation methods in Chemical Physics: Theory and application, ISBN: 978-0-470-02938-1*; Mennucci, B., Cammi, R., Eds.; Wiley: New York, 2007; pp 252−264.
(68) Bak, K. L.; Hansen, A. E.; Ruud, K.; Helgaker, T.; Olsen, J.; Jørgensen, P. *Theor. Chim. Acta* **1995**, *90*, 441.
(69) Note the extra factor of 3/4 with respect to ref 44, due to a different definition of the rotational strength ^{I}R of our eq 6.
(70) Pecul, M.; Ruud, K.; Helgaker, T. *Chem. Phys. Lett.* **2004**, *388*, 110.
(71) London, F. *J. Phys. Radium* **1937**, *8*, 397.
(72) Frisch, M. J.; Trucks, G. W.; Schlegel, H. B.; Scuseria, G. E.; Robb, M. A.; Cheeseman, J. R.; Montgomery, J. A., Jr.; Vreven, T.; Kudin, K. N.; Burant, J. C.; Millam, J. M.; Iyengar, S. S.; Tomasi, J.; Barone, V.; Mennucci, B.; Cossi, M.; Scalmani, G.; Rega, N.; Petersson, G. A.; Nakatsuji, H.; Hada, M.; Ehara, M.; Toyota, K.; Fukuda, R.; Hasegawa, J.; Ishida, M.; Nakajima, T.; Honda, Y.; Kitao, O.; Nakai, H.; Klene, M.; Li, X.; Knox, J. E.; Hratchian, H. P.; Cross, J. B.; Bakken, V.; Adamo, C.; Jaramillo, J.; Gomperts, R.; Stratmann, R. E.; Yazyev, O.; Austin, A. J.; Cammi, R.; Pomelli, C.; Ochterski, J. W.; Ayala, P. Y.; Morokuma, K.; Voth, G. A.; Salvador, P.; Dannenberg, J. J.; Zakrzewski, V. G.; Dapprich, S.; Daniels, A. D.; Strain, M. C.; Farkas, O.; Malick, D. K.; Rabuck, A. D.; Raghavachari, K.; Foresman, J. B.; Ortiz, J. V.; Cui, Q.; Baboul, A. G.; Clifford, S.; Cioslowski, J.; Stefanov, B. B.; Liu, G.; Liashenko, A.; Piskorz, P.; Komaromi, I.; Martin, R. L.; Fox, D. J.; Keith, T.; Al-Laham, M. A.; Peng, C. Y.; Nanayakkara, A.; Challacombe, M.; Gill, P. M. W.; Johnson, B.; Chen, W.; Wong, M. W.; Gonzalez, C.; Pople, J. A. *GAUSSIAN 03*, revision A.1; Gaussian, Inc.: Pittsburgh, PA, 2003.
(73) Norman, P.; Jonsson, D.; Ågren, H.; Dahle, P.; Ruud, K.; Helgaker, T.; Koch, H. *Chem. Phys. Lett.* **1996**, *253*, 1.
(74) Fossgård, E.; Ruud, K. *J. Comput. Chem.* **2006**, *27*, 326.
(75) *DALTON, a molecular electronic structure program*, release 2.0; 2005, see http://www.kjemi.uio.no/software/dalton/dalton.html.
(76) Auer, H. *J. Am. Chem. Soc.* **1973**, *95*, 3003.
(77) Available Supporting Information.
(78) Peach, M. J. G.; Benfield, P.; Helgaker, T.; Tozer, D. J. *J. Chem. Phys.* **2008**, *128*, 044118.
(79) Peach, M. J. G.; Le Sueur, C. R.; Ruud, K.; Guillaume, M.; Tozer, D. J. *Phys. Chem. Chem. Phys.* **2009**, *11*, 4470.
(80) Skomorowski, W.; Pecul, M.; Salek, P.; Helgaker, T. *J. Chem. Phys.* **2007**, *127*, 085102.
(81) Pecul, M.; Ruud, K.; Rizzo, A.; Helgaker, T. *J. Phys. Chem. A* **2004**, *108*, 4269.
(82) Marchesan, D.; Coriani, S.; Forzato, C.; Nitti, P.; Pitacco, G.; Ruud, K. *J. Phys. Chem. A* **2005**, *109*, 1449.

JP1004659